

A minimal model for flow control on an aerofoil using a poro-elastic coating



Divya Venkataraman^{a,*}, Alessandro Bottaro^a, Rama Govindarajan^{b,1}

^a Department of Civil, Chemical & Environmental Engineering, University of Genova, Italy

^b Centre for Interdisciplinary Sciences, Tata Institute of Fundamental Research, Hyderabad, India

ARTICLE INFO

Article history:

Received 21 August 2013

Received in revised form

12 February 2014

Accepted 17 February 2014

Available online 21 March 2014

Keywords:

Flow control

Poro-elastically coated aerofoil

Biomimetics

ABSTRACT

A minimal model is obtained for vortex-shedding from an aerofoil with a porous coating of flow-compliant feather-like actuators, in order to better understand this passive way to achieve flow control. This model is realized by *linearly* coupling a minimal-order model for vortex-shedding from the same aerofoil *without* any such coating with an equation for the poro-elastic coating, here modelled as a linear damped oscillator. The various coefficients in this model, derived using perturbation techniques, aid in our understanding of the physics of this fluid–structure interaction problem. The minimal model for a coated aerofoil indicates the presence of distinct regimes that are dependent on the flow and coating characteristics. The models and the parametric studies performed provide insight into the selection of optimal coating parameters, to enable flow control at low Reynolds numbers.

© 2014 Elsevier Ltd. All rights reserved.

1. Introduction

The objective of this paper is to derive a minimal model for the vortex-shedding behind a symmetric aerofoil, a part of which is covered with a poro-elastic coating of *passive* flow-compliant feathers, the aerofoil being oriented at an angle to the free stream in a laminar flow regime. Such a minimal model is realized by *linearly* coupling the minimal-order model for the vortex-shedding (expressed in terms of an integral quantity such as the lift coefficient) behind the same aerofoil *without* such a coating (henceforth referred to as “smooth”), with an equation which describes the dynamics of the porous, compliant coating, here modelled as a linear damped oscillator. The basic motivation for developing and studying a minimal model in this manner is that, although numerical as well as experimental parametric studies for such a class of passive flow control techniques involving shape-optimization have been performed in the recent past (including but not limited to [Bechert et al., 1997](#); [Bakhtian et al., 2007](#); [Favier et al., 2009](#); [Brücker, 2011](#); [Lam et al., 2012](#); [Venkataraman and Bottaro, 2012](#); [Igbalajobi et al., 2013](#); [Brücker and Weidner, 2013](#)), a theoretical model can help in better understanding the underlying physics of this coupled fluid–structure interaction problem without the need for performing extensive time-consuming computations and/or experiments. At this point, it is pertinent to note that some theoretical studies have also been performed recently for fluid–structure interaction problems, but for simpler flow conditions (such as that of a potential flow in a channel bounded by cantilever beams, [Jang et al., 2013](#)).

* Corresponding author.

E-mail address: vdivya8@yahoo.co.in (D. Venkataraman).

¹ On lien from the Jawaharlal Nehru Centre for Advanced Scientific Research, Bangalore, India.

Studies of this passive flow control technique were initially motivated from the “pop-up” of covert feathers present at the roots of the wings of some birds, which automatically become active during flow regimes involving high angle of attack, such as perching manoeuvres. In particular, many experimental studies, such as [Bechert et al. \(1997\)](#) and [Bakhtian et al. \(2007\)](#), have proved the effectiveness of such feathers in applications including drag reduction and delay in stall angles. Suitable implementations of such passive flow control techniques can also be potentially beneficial for technological applications based on micro-aerial vehicles, where it is very crucial to balance aerodynamic performance and manoeuvring capabilities on one hand against constraints of payload that typically also include flow control appendages. More generally, several studies have also been performed for vortex-shedding behind cylinders (which are typical examples of bluff bodies), particularly in the context of active flow control techniques such as regulated oscillations in the streamwise or cross-flow directions ([Xu et al., 2006](#); [Perdikaris et al., 2009](#); [Srikanth et al., 2011](#)), to desirably manipulate the flow field in the vicinity of the body.

The importance of reduced-order models, in particular for problems such as the one considered in this paper, is that they have a two-fold advantage over their counterparts which rely on time-consuming computations. In such contexts, low-order models become pertinent when very complex as well as computationally expensive numerical simulations of fluid flow, as well as extensive parametric studies performed in the course of such studies would need more efficient, reliable and low-cost replacements. Studies on developments of low-order models for cylinders which are free to move in one direction but constrained in others have been performed in the past ([Gaster, 1969](#)), particularly vis-a-vis determining the conditions under which vortex-induced vibrations can take place and thus, how they can possibly be controlled ([Hartlen and Currie, 1970](#); [Currie and Turnbull, 1987](#)). Such theoretical models also yield useful insights into how and why the flow characteristics change with different control parameters/coating properties and hence have the capability to predict “optimal” parameters. This paper is in fact a first step towards addressing the issue of rigorously and theoretically characterizing *passive* flow-control/actuator parameters which should as well as should not be used, to obtain favourable modifications in the flow field.

This paper begins with a description of the minimal model for a coated aerofoil, starting with a derivation of the closed-form expression for the solution of such a coupled system, in [Section 2](#). [Section 3](#) derives the expressions for the parameters of the minimal model in terms of results from the full computational model, along the lines of what was done for the minimal model for vortex-shedding behind a smooth aerofoil ([Venkataraman, 2013](#)). [Section 4](#) presents an overview of simulations performed with the full computational model, to arrive at the minimal model. In order to better understand the physics, the first part of this section presents results from prototype simulations, obtained by considering the flow over a flat plate, both aligned with the free-stream as well as oriented at an incidence angle to it. The second part of this section presents results for the case of the symmetric aerofoil at an angle of attack to the free stream, and correlates the results for the flat plate with those of the aerofoil, thus presenting reasons for developing the specific minimal model for the coupled system. [Section 5](#) compares the results from the full computational model for the aerofoil with those obtained from the minimal model (as outlined in [Sections 2](#) and [3](#)), hence proving the effectiveness of the minimal model, while [Section 6](#) presents parametric studies for qualitative changes in characteristics of solutions for the coupled system. Finally [Section 7](#) summarizes the paper and lists some perspectives for future work.

2. Linear minimal model for coupled fluid–structure interaction: derivation of solution

To follow the simplest approach, we consider the reduced-order model for the feathery coating as a linear spring (where each feather in the coating is taken to be a rigid beam ([Venkataraman and Bottaro, 2012](#); [Venkataraman et al., 2013](#)), described by a linear damped oscillator's equation

$$\ddot{\theta} + c\dot{\theta} + \omega_1^2\theta = 0, \quad (2.1)$$

where ω_1^2 is the (positive) stiffness constant of the linear spring and c is its damping coefficient. It must be noted here that the oscillations of such a *standalone* linear spring asymptotically die out or amplify depending on whether c is positive or negative. However when an external forcing is applied to such an independent oscillator (via a non-zero term on the right hand side of Eq. (2.1)), its asymptotic dynamics will also depend on this external forcing.

Here θ is a variable that measures the dynamics of this poro-elastic coating and may possibly denote one of the following:

1. If the coating is not strictly a “dense continuum” of feathers – each feather in this coating is sufficiently far apart from its neighbour so as to not affect its dynamics and in turn, not get affected by this neighbour's dynamics (compare also [Brücker and Weidner, 2013](#)) – then, θ can denote the angular displacement of each such feather about its angular mean/equilibrium position θ_{eq} . Thus, interaction moments between neighbouring feathers ([Favier et al., 2009](#); [Venkataraman and Bottaro, 2012](#)) are not significant. Further, c and ω_1 denote the dissipation constant and the spring constant respectively, for each of these feathers. In this case, we postulate that the individual elements of the coating have *synchronous* dynamics.

Alternatively, Eq. (2.1) can also be interpreted to measure the dynamics of a single self-actuated movable flap, rather than a cluster of feathers.

2. In the spirit of generalizing the study to a “dense” coating and also of developing a *minimal* model for this coupled fluid–structure interaction problem, θ can be interpreted as the displacement of the fluid-coating interface from an equilibrium position, as shown in [Fig. 1](#). It is re-emphasized here that in this case, the structure model equation (2.1) does

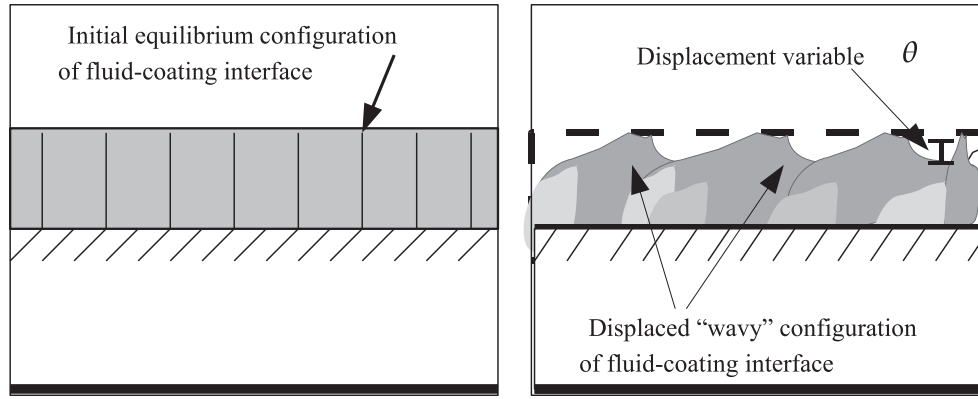


Fig. 1. Fluid-coating interface: (left) initial undisturbed configuration (i.e., without any forcing from the fluid), the vertical lines here denote a discrete number of feathers spread uniformly in this coating; (right) disturbed configuration showing the displacement variable θ . Note here that the colour gradient in this disturbed coating characterizes the non-uniform, time-varying porosity (i.e., darker shades denote clustering of feathers while lighter shades stand for areas with a lower instantaneous concentration of feathers).

not govern the dynamics of the angular displacements of the individual feathers but the *overall* displacement of the coating as a whole. Hence, again interaction effects can be neglected in the *overall* structure model.

When Eq. (2.1) is coupled with the minimal model for vortex-shedding behind a smooth aerofoil (as captured by the aerofoil's lift and derived in Venkataraman, 2013), given by

$$\ddot{C}_L + \omega^2 C_L - \omega^2 \tilde{C}_L - \mu \dot{C}_L + \alpha (\dot{C}_L)^3 - \beta (\dot{C}_L)^2 = 0, \quad (2.2)$$

where all the model parameters ω^2 , μ , α and β are positive (cf. Venkataraman, 2013), the coupled system is given by

$$\ddot{C}_L + \omega^2 C_L - \omega^2 \tilde{C}_L - \mu \dot{C}_L + \alpha (\dot{C}_L)^3 - \beta (\dot{C}_L)^2 = \rho_1 \theta; \quad (2.3)$$

$$\ddot{\theta} + c\dot{\theta} + \omega_1^2 \theta = \rho_2 (C_L - \tilde{C}_L), \quad (2.4)$$

where \tilde{C}_L is the time-averaged mean value of the lift coefficient for the smooth aerofoil (Venkataraman, 2013), and ρ_1 and ρ_2 are constants enforcing a linear coupling between the fluid and structure systems, both of which could be either positive or negative. It is interesting to note here that since the structure-to-fluid forcing is itself directly proportional to the displacement of the coating interface θ via the coupling parameter ρ_1 , this parameter can be physically interpreted as (a function of) the density/porosity of the feathery coating. That is, as the porosity of the coating decreases (or equivalently its density increases), the magnitude of the structure-to-fluid forcing increases. Similarly, since the fluid-to-structure forcing (i.e., right hand side of Eq. (2.4)) determines the qualitative nature of oscillations of the structure with its amplitude also governed by the coupling parameter ρ_2 , this parameter can be physically interpreted as (a function of) the compliance of the feathers in the coating. That is, compliance of the poro-elastic coating increases as the parameter ρ_2 is increased.

It must also be noted here that although the structure model as well as the couplings between the fluid and structure components are linear, the whole coupled system capturing vortex-shedding from a *poro-elastically coated* aerofoil continues to remain non-linear, exactly as in the case of a *smooth* aerofoil. This is because the non-linearities in the hydrodynamics (as in the left hand side of (2.3)) and consequently the fluid-to-structure forcing (in the right hand side of (2.4)) are the drivers of the system – it is only the spring response (left hand side of (2.4)) which is linear.

As done before for the case of smooth aerofoil, this coupled system can be solved by the method of multiple scales (Van Dyke, 1964; Strogatz, 1994; Rand, 2012), to find the general form of the solution, C_L and θ , in terms of its model parameters. Conversely, given the form of the solution (for instance from the computational data, as in the present case), it is possible to find the parameters of the minimal model in terms of the numerical/physical characteristics of the results from the computational model. In addition, it is also possible to make some inferences about “optimal” structure model parameters that yield the desired behaviour for the solution of the coupled system.

Following the method used for the flow around a smooth aerofoil (Venkataraman, 2013), we consider the coupled problem when the damping and nonlinearities for the fluid component, the damping/dissipation for the structure component as well as the coupling between the fluid and structure parts are weak. Thus, by taking μ , α , β , c , ρ_1 and ρ_2 all to be of $O(\delta)$ (where δ is a bookkeeping parameter that measures how strong the non-linearity in the system is, $\delta \ll 1$), we determine a second-order approximate solution in δ for the lift coefficient and the angular displacement of the reference feather. The fact that all the fluid as well as structure damping terms and fluid–structure coupling terms are of $O(\delta)$ which physically means that all these damping and coupling effects are *weak* compared to the oscillation effects of the two *stand-alone* fluid and structure components of this coupled fluid–structure system.

Eqs. (2.3) and (2.4) are solved by first transforming them into two complex-valued first-order equations, in variables ζ_1 and ζ_2 . Then introducing the fast, slow and slower time scales, given by $T_0 = t$, $T_1 = \delta t$, and $T_2 = \delta^2 t$, respectively, using the expansions $\zeta_1 = \sum_{j=0}^2 \delta^j \zeta_{1,j}(T_0, T_1, T_2) + O(\delta^3)$; and $\zeta_2 = \sum_{j=0}^2 \delta^j \zeta_{2,j}(T_0, T_1, T_2) + O(\delta^3)$ in these complex-valued first-order equations, and separating coefficients of like powers of δ yields three ordinary differential equations each for ζ_1 (involving $\zeta_{1,0}$,

$\zeta_{1,1}$ and $\zeta_{1,2}$) and ζ_2 (involving $\zeta_{2,0}$, $\zeta_{2,1}$ and $\zeta_{2,2}$). Both these systems of equations can be solved for ζ_1 and ζ_2 . The solutions involve arbitrary functions $A_1(T_1, T_2)$ and $A_2(T_1, T_2)$, in terms of the time scales T_1 and T_2 (but constant with respect to the time scale T_0), and to ensure bounded solutions (by eliminating secular terms), four solvability conditions are obtained (involving $\partial A_1/\partial T_1$, $\partial A_1/\partial T_2$, $\partial A_2/\partial T_1$ and $\partial A_2/\partial T_2$). Finally using the polar transformations $A_1(t) = a_1(t)e^{i\gamma_1(t)}/2$ and $A_2(t) = a_2(t)e^{i\gamma_2(t)}/2$ in the expressions for $C_L(t)$ and $\theta(t)$ respectively, the following closed-form solutions for the *modified* lift coefficient is obtained

$$C_L(t) = \tilde{C}_L + \frac{\delta\beta}{2} a_1^2(t) + a_1(t) \sqrt{1 + \left[\frac{3}{16} \delta\alpha\omega a_1^2(t) - \frac{\delta\mu}{4\omega} \right]^2} \sin [\omega t + \gamma_1(t) + \eta_1] + \frac{\delta\beta}{6} a_1^2(t) \cos (2[\omega t + \gamma_1(t)]) + \frac{\delta\alpha}{32} \omega a_1^3(t) \sin (3[\omega t + \gamma_1(t)]) + \frac{\delta\rho_1}{(\omega - \omega_1)(\omega + \omega_1)} a_2(t) \cos [\omega_1 t + \gamma_2(t)]; \tag{2.5}$$

while the fluid-coating interface solution reads

$$\theta(t) = a_2(t) \sqrt{1 + \frac{\delta^2 c^2}{16\omega_1^2}} \sin [\omega_1 t + \gamma_2(t) + \eta_2] - \frac{\delta\rho_2}{(\omega - \omega_1)(\omega + \omega_1)} a_1(t) \cos [\omega t + \gamma_1(t)], \tag{2.6}$$

where $\eta_1(t) = \tan^{-1}\{16\omega/[\delta(3\alpha\omega^2 a_1^2(t) - 4\mu)]\}$ and $\eta_2(t) = \tan^{-1}\{4\omega_1/c\}$.

Combining the solvability conditions corresponding to A_1 with the polar transformation above for A_1 , the following modulation equations arise:

$$\dot{a}_1(t) = \frac{\delta}{2} \left\{ \frac{\mu}{2} a_1(t) - \frac{3}{8} \alpha\omega^2 a_1^3(t) \right\}; \tag{2.7}$$

$$\dot{\gamma}_1(t) = -\delta^2 \left\{ \frac{\mu^2}{8\omega} + \frac{3}{16} \mu\alpha\omega a_1^2(t) - \frac{\beta^2}{6} \omega a_1^2(t) - \frac{27}{256} \alpha^2 \omega^3 a_1^4(t) - \frac{\rho_1\rho_2}{2\omega(\omega - \omega_1)(\omega + \omega_1)} \right\}, \tag{2.8}$$

and likewise for A_2

$$\dot{a}_2(t) = -\frac{\delta}{2} c a_2(t); \tag{2.9}$$

$$\dot{\gamma}_2(t) = -\delta^2 \left\{ \frac{ic^2}{8\omega_1} + \frac{\rho_1\rho_2}{2\omega_1(\omega - \omega_1)(\omega + \omega_1)} \right\}. \tag{2.10}$$

Again under the initial assumption that $C_L(t)$ and $\theta(t)$ both have reached their equilibrium states, Eqs. (2.7) and (2.9) can be solved. This results in two possible values of a_1 : 0 and $(2/\omega)\sqrt{\mu/3\alpha}$ (exactly as in the calculations for the case of smooth aerofoil, Venkataraman, 2013). Further, the only possibilities for steady-state condition for $a_2(t)$ are $c=0$ or $a_2(t)=0$. The trivial solution of both $a_1(t)=0$ and $a_2(t)=0$ can be ruled out. The other three cases are the following:

Case 1 - Weak structure-to-fluid coupling: $a_1(t) = (2/\omega)\sqrt{\mu/3\alpha}$ and $a_2(t) \equiv 0$. The possibility of $a_2(t)$ being *identically zero* physically means that the dissipation constant c of the reference feather is allowed to be *arbitrarily large*, and hence, the oscillations of the *independent* structure part die out almost instantly once a steady state is reached. As a result, for this case, in the two-way coupled fluid–structure system, the dynamics of the structure part has exactly the same frequency as the fluid part, this frequency being given by $\omega_{s,1} = \omega + \gamma_1$ (as calculated below).

Also, the non-zero value of a_1 forces the phase angle η_1 to be $\pi/2$, and

$$\dot{\gamma}_1(t) = -\delta^2 \left\{ \frac{\mu^2}{16\omega} - \frac{2\beta^2\mu}{9\alpha\omega} - \frac{\rho_1\rho_2}{2\omega(\omega - \omega_1)(\omega + \omega_1)} \right\}. \tag{2.11}$$

Further, as $c \rightarrow \infty$, $\eta_2 \rightarrow 0$ and $\dot{\gamma}_2(t) \rightarrow \infty$. Thus, Eq. (2.5) *degenerates* to an equation similar in form to the equation for the lift coefficient of a smooth aerofoil (cf. Venkataraman, 2013), but with a different ω_s , while (2.6) simplifies to

$$\theta(t) = -\frac{2\delta\rho_2}{\omega(\omega - \omega_1)(\omega + \omega_1)} \sqrt{\frac{\mu}{3\alpha}} \cos (\omega_{s,1} t), \tag{2.12}$$

where $\omega_{s,1} = \omega - (\delta\mu)^2/(16\omega) - 2(\delta\beta)^2\mu/(9\alpha\omega) - (\delta\rho_1)(\delta\rho_2)/[2\omega(\omega - \omega_1)(\omega + \omega_1)]$.

It must be noted that with such a coating, the lift of the aerofoil $C_L(t)$, under steady-state conditions, displays exactly the same characteristics in its dynamics (such as the presence of second and third super-harmonics of the fundamental frequency $\omega_{s,1}$) as in the case when the aerofoil is not coated with any feathers (Venkataraman, 2013). However, the displacement variable of the coating $\theta(t)$ exhibits just one frequency, equal to the fundamental frequency $\omega_{s,1}$.

Case 2 – Weak fluid-to-structure coupling: $a_1(t) \equiv 0$ and $c=0$. In this case, owing to the fact that the dissipation constant c vanishes, $a_2(t)$, in its steady state, is allowed to be an arbitrary constant C_0 , either small or large. This case turns out to be similar to case 1, where the dynamics of fluid and structure happens at the same frequency, now given by $\omega_{s,2} = \omega_1 + \gamma_2$.

Also, since $a_1(t) \equiv 0$, $\eta_1 = \tan^{-1}\{-4\omega/(\delta\mu)\}$ whose limit is $\pi/2$ as $\delta \rightarrow 0$. Further, $\gamma_1(t) = -\delta^2\{\mu^2/(8\omega) - \rho_1\rho_2/[2\omega(\omega - \omega_1)(\omega + \omega_1)]\}$. Besides, since $c=0$, $\eta_2 = \pi/2$ and

$$\gamma_2(t) = -\delta^2 \left\{ \frac{\rho_1\rho_2}{2\omega_1(\omega - \omega_1)(\omega + \omega_1)} \right\}. \tag{2.13}$$

Thus, Eq. (2.5) simplifies to

$$C_L(t) = \tilde{C}_L + \frac{\delta\rho_1 C_0}{(\omega - \omega_1)(\omega + \omega_1)} \cos(\omega_{s,2}t), \tag{2.14}$$

while Eq. (2.6) simplifies to

$$\theta(t) = C_0 \cos(\omega_{s,2}t), \tag{2.15}$$

where $\omega_{s,2}$ is given by $\omega_1 - (\delta\rho_1)(\delta\rho_2)/[2\omega_1(\omega - \omega_1)(\omega + \omega_1)]$.

In this case, it must be noted that both the dynamics of the lift $C_L(t)$ as well as the displacement variable of the coating $\theta(t)$ exhibit the same frequency $\omega_{s,2}$, and no super-harmonics are observed in either case.

Case 3 – Two-way coupling: $a_1(t) = (2/\omega)\sqrt{\mu/(3\alpha)}$ and $c=0$. In this case, Eq. (2.5) simplifies to

$$C_L(t) = \tilde{C}_L + \frac{2\delta\beta\mu}{3\alpha\omega^2} + \sqrt{\frac{4\mu}{3\alpha\omega^2}} \cos(\omega_{s,1}t) + \frac{2\delta\beta\mu}{9\alpha\omega^2} \cos(2\omega_{s,1}t) + \delta\sqrt{\frac{\mu^3}{432\alpha\omega^4}} \sin(3\omega_{s,1}t) + \frac{\delta\rho_1 C_0}{(\omega - \omega_1)(\omega + \omega_1)} \cos(\omega_{s,2}t), \tag{2.16}$$

while Eq. (2.6) simplifies to

$$\theta(t) = C_0 \cos(\omega_{s,2}t) - \frac{2\delta\rho_2}{\omega(\omega - \omega_1)(\omega + \omega_1)} \sqrt{\frac{\mu}{3\alpha}} \cos(\omega_{s,1}t), \tag{2.17}$$

where $\omega_{s,1}$ and $\omega_{s,2}$ are given, as before, from cases 1 and 2 respectively. It is emphasized here that the last term in (2.16), $\{\delta\rho_1 C_0/[(\omega - \omega_1)(\omega + \omega_1)]\} \cos(\omega_{s,2}t)$ is precisely the component of the lift exclusively associated with the structural coupling. It must, hence, be noted that only in case 1 (where there is weak structure-to-fluid coupling), this term vanishes, whereas in the other two cases this term is non-zero.

Here, it can be seen that, in general, $\omega_{s,1}$ and $\omega_{s,2}$ are two distinct frequencies. Hence, in this case, the two-way coupled fluid–structure interaction displays very rich dynamics, where for one frequency super-harmonics can be observed, while for the other no such super-harmonics are present.

It must be noted here that in all the above closed-form solutions, the amplitude of oscillations of the structure corresponding to the frequency $\omega_{s,1}$ (which in fact is the frequency obtained by modifying the coefficient ω in the equation of the stand-alone fluid part in the coupled system, as can be seen from Eq. (2.12)) is of $O(\delta)$. However, the amplitude of oscillations of the lift coefficient corresponding to this same frequency is of $O(1)$. This phenomenon can be physically interpreted in the form that the magnitude of the wavy displacement of the fluid–coating interface corresponding to this primary frequency will understandably be of smaller order than the magnitude of oscillations of the lift coefficient, since it has been assumed from the beginning that the fluid-to-structure coupling coefficient ρ_2 is of $O(\delta)$. This observation further justifies the appropriateness of modelling the dynamics of the poro-elastic coating by means of the vertical displacement of the coating interface (rather than by the angular displacement of each feather in the coating), since the displacement of the coating interface will always be typically less than the oscillations/displacements of individual feathers. Such a conclusion based on order-of-magnitude analysis need not be true in general if, for instance, the magnitude of some coupling parameter is increased from the present $O(\delta)$ to $O(1)$.

Table 1
Effect of change in coating parameters on characteristics of lift coefficient.

Case	Resonant frequency conditions	Non-resonant frequency conditions
1: Weak structure-to-fluid coupling	$\sqrt{\frac{4\mu}{3\alpha\omega^2}}$ dominates mean lift increase	Changes in coating parameters do not directly affect lift characteristics
2: Weak fluid-to-structure coupling	Mean lift increase by $O(\delta)$ when: (a) structure–fluid coupling parameter ρ_1 increased; (b) compliance is increased so that the amplitude of steady-state oscillations of feather C_0 is large	Lift fluctuations decrease if $\frac{\delta\rho_1 C_0}{(\omega - \omega_1)(\omega + \omega_1)} < \sqrt{\frac{4\mu}{3\alpha\omega^2}}$
3: Two-way coupling	Same as case 2	Lift fluctuations increase avoided if $\frac{\delta\rho_1 C_0}{(\omega - \omega_1)(\omega + \omega_1)} < \sqrt{\frac{4\mu}{3\alpha\omega^2}}$

In all the above three cases, we can have the possibilities of at least one of $\omega_{s,1}$ or $\omega_{s,2}$ being zero. It is important to note that if $\omega_{s,1}$ is zero, then so is $\omega_{s,2}$ and vice-versa. This is because if $\omega_{s,1}$ is zero (in which case, $\omega_s = (\delta\rho_1)(\delta\rho_2)/[2\omega(\omega - \omega_1)(\omega + \omega_1)]$, where it must be recalled that ω_s is the vortex-shedding frequency for the *smooth* aerofoil), the right-hand side of the above condition must be of $O(1)$, since ω_s is itself of $O(1)$. This is possible only if $\omega \sim \omega_1$, which is nothing but the *resonant* condition for the coupled fluid–structure system. Under this condition, it can be easily seen that $\omega_{s,2}$ is also zero, since $\omega_1 = (\delta\rho_1)(\delta\rho_2)/[2\omega_1(\omega - \omega_1)(\omega + \omega_1)]$ by similar order of magnitude analysis, as presented above. The other possibility is the *non-resonant* condition, where both $\omega_{s,1}$ or $\omega_{s,2}$ are non-zero. A summary of the effects produced on the characteristics of the lift coefficient (in the form of change in mean lift or change in lift fluctuations about this mean) is presented in Table 1.

3. Structure and coupling parameters from results of computational model

The calculations in this section are analogous to those of the smooth aerofoil (Venkataraman, 2013). Thus, the aim in this section is to derive mathematical expressions for the fluid parameters $\omega, \mu, \alpha, \beta$; the structure parameters ω_1 and c ; and the fluid–structure coupling parameters ρ_1 and ρ_2 ; in terms of the characteristics of the results from the full computational model for the poro-elastically coated aerofoil, so that the best possible fit for the numerical data is obtained.

If one considers the most generic analytical form of the solution for the lift coefficient $C_L(t)$ and the displacement of the fluid–coating interface θ , given by Eqs. (2.5) and (2.6), it can be seen that under steady state assumptions for the amplitudes of $C_L(t)$ and θ , these equations reduce to Eqs. (2.16) and (2.17). Eqs. (2.16) and (2.17) are now re-written as

$$C_L(t) = \tilde{C}_L + l_1 \cos(\omega_{s,1}t) + l_2 \cos(2\omega_{s,1}t) + l_3 \sin(3\omega_{s,1}t) + l'_1 \cos(\omega_{s,2}t); \tag{3.1}$$

$$\theta(t) = \theta_1 \cos(\omega_{s,2}t) + \theta'_1 \cos(\omega_{s,1}t), \tag{3.2}$$

where $l_1, l_2, l_3, l'_1, \omega_{s,1}, \theta_1, \theta'_1$ and $\omega_{s,2}$ are eight quantities which can be recovered from computational data, and depend on the eight unknown model parameters $\omega, \delta\mu, \delta\alpha, \delta\beta, \delta\rho_1, \omega_1, \delta c$ (or equivalently C_0) and $\delta\rho_2$. Hence, solving these unknowns yields the following two coupled quadratic equations for ω and ω_1 :

$$(l_1^2 l_3 - 36l_3^3 - 6l_2^2 l_3)\omega^2 - l_1^2 l_3 \omega_{s,1} \omega - l_1^2 l_3 \omega_1^2 + l_1^2 l_3 \omega_{s,2} \omega_1 = 0; \tag{3.3}$$

$$(2\theta_1 l_1 - l'_1 \theta'_1)\omega_1^2 - 2\omega_{s,2} \theta_1 l_1 \omega_1 + l'_1 \theta'_1 \omega^2 = 0; \tag{3.4}$$

and the following six equations for the remaining parameters:

$$\delta\mu = \frac{24l_3\omega}{l_1}; \tag{3.5}$$

$$\delta\alpha = \frac{32l_3}{l_1^3\omega}; \tag{3.6}$$

$$\delta\beta = \frac{6l_2}{l_1^2}; \tag{3.7}$$

$$C_0 = \theta_1; \tag{3.8}$$

$$\delta\rho_1 = \frac{(\omega - \omega_1)(\omega + \omega_1)l'_1}{C_0}; \tag{3.9}$$

$$\delta\rho_2 = \frac{-\omega(\omega - \omega_1)(\omega + \omega_1)\theta'_1}{2} \sqrt{\frac{3\alpha}{\mu}}. \tag{3.10}$$

It must be noted here that Eqs. (3.5) and (3.6) involve ω while Eqs. (3.9) and (3.10) involve both ω as well as ω_1 , which can be solved from the coupled system of quadratic equations (3.3) and (3.4).

4. Overview of simulations

4.1. Prototype simulations: case of flat plate

Case A: Flat plate aligned with the free-stream. In order to relate the theoretical results obtained in Sections 2 and 3 to the results from the full computational model for the symmetric aerofoil (presented in the second part of this section), the flow configuration is initially taken to be simpler, and the flow over a flat plate, with rounded leading and trailing edges, aligned with the free-stream is considered. The computational model employed here for the fluid domain is based on directly resolving the continuity and momentum equations (for an incompressible flow regime) on a Cartesian grid in a two-dimensional domain, with the use of the immersed boundary method. Neumann outflow boundary condition is used in the

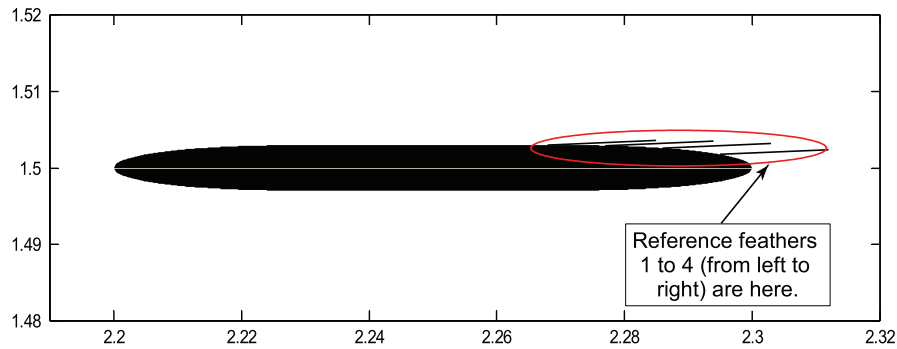


Fig. 2. Placement of the poro-elastic coating on the horizontal flat plate, depicted by the reference feathers (shown here by the horizontal, black lines towards the end of the top side of the flat plate).

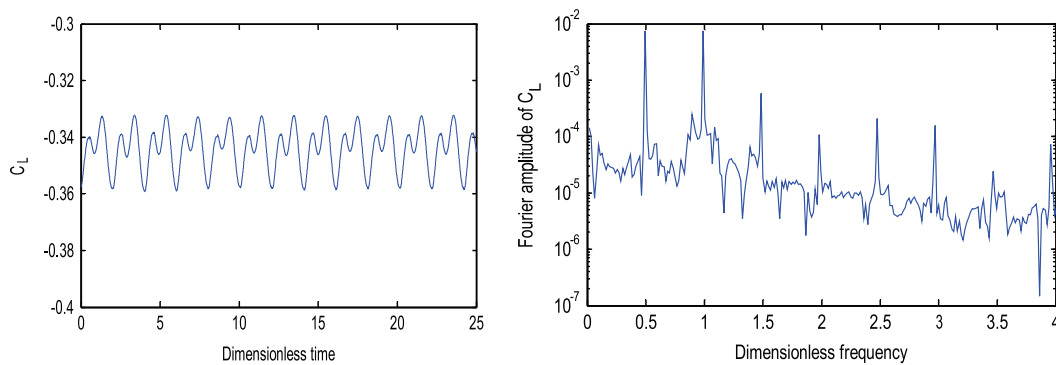


Fig. 3. (Left) Time evolution of the lift coefficient for the horizontal flat plate with a poro-elastic coating over the end of its top side; (right) Fourier spectrum of the lift coefficient shown in the left frame.

streamwise direction so as to ensure that no extraneous frequency enters the domain inlet. The dynamics of the poro-elastic coating is approximated from the dynamics of a discrete number of *reference* feathers homogeneously spread over the dense coating. These reference feathers are taken to be rigid beams behaving as linear damped oscillators interacting with each other via forces analogous to those in damped springs. Further details of the computations can be referred to in Venkataraman and Bottaro (2012) and Venkataraman (2013). The plate considered for these prototype simulations is shown in Fig. 2. The simulations developed here provide a good prototype flow for us to understand the mechanisms of lift enhancement or drag reduction.

A flat plate at zero angle of attack without any poro-elastic coating has no mean lift because of symmetry of the flow around it (which is also confirmed from simulations). To see what changes are introduced in the flow by using the poro-elastic coating, the flat plate is coated with such flow-compliant feathers towards the end of its top side, whose dynamics are approximated by a certain number of *reference* feathers, as shown by the schematic diagram in Fig. 2. As explained before in earlier work (Venkataraman and Bottaro, 2012), since the rigidity moment dominates the angular dynamics of the feathers, the dimensionless *linear* structure frequency is taken to be the dimensionless *linear* rigidity frequency (non-dimensionalised by the time scale given by the ratio between the free-stream speed and the length of the flat plate, which in this case is 1.65), and is given by $1/(2\pi \times 1.65) \sqrt{K_r/Ml_c^2}$, where K_r , M and l_c are the rigidity modulus, mass and half-length of each reference feather, with non-dimensional values 8.33, 5.5 and 8.5×10^{-2} , respectively (obtained by following the normalization procedure in Venkataraman and Bottaro, 2012). In the present case, this dimensionless linear structure frequency f_s is 0.4594.

Fig. 3 shows the dynamics of the lift coefficient for this poro-elastically coated flat plate, while Fig. 4 shows the dynamics of the four reference feathers that approximate the dynamics of the coating. Both these figures are shown in the time as well as frequency domains.

From the left frame of Fig. 3, it can be clearly seen that with the present selection of structure parameters and their placement on the flat plate, a large negative lift is produced. This is, in general, because these feathers introduce asymmetry in the pressure distribution between the top and bottom surfaces of the flat plate. Thus, by arguments of symmetry, it can be argued that if a poro-elastic coating with the same structure parameters was used only on the bottom side of the flat plate, but over the same horizontal extent, then a large positive lift would be produced.

Again from the left frame of Fig. 3, it can be clearly seen that the poro-elastic coating introduces some periodicity in the flow and makes the flow unsteady, by triggering vortex-shedding. From the right frame of Fig. 3, it can be seen that the Fourier spectrum has a *unique* fundamental frequency (coinciding with the frequency of vortex-shedding) equal to 0.4947 along with all its super-harmonics.

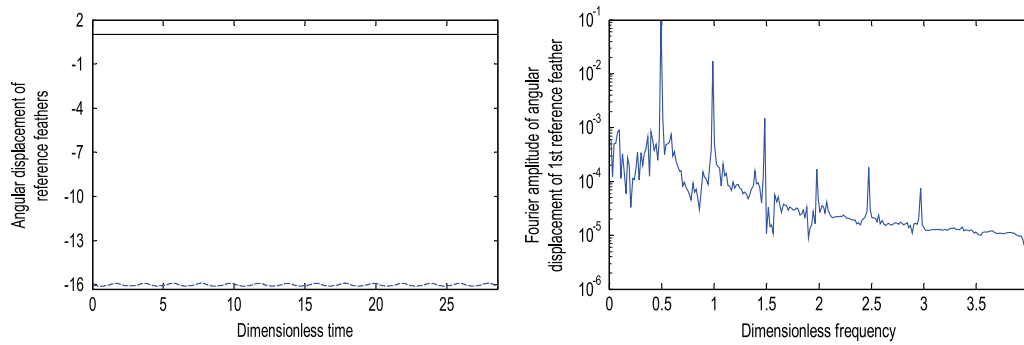


Fig. 4. (Left) Time evolution of the angular displacement of the reference feathers, corresponding to the case shown in Fig. 3 (i.e., for the horizontal flat plate). The blue dashed curve shows the dynamics of feather 1 (closest to the leading edge of the plate) while the solid, black curve shows the dynamics of feathers 2, 3, and 4 (progressively farther away from the leading edge), all of which are seen to be identical; (right) Fourier spectrum of the angular displacement of feather 1. (For interpretation of the references to colour in this figure caption, the reader is referred to the web version of this paper.)

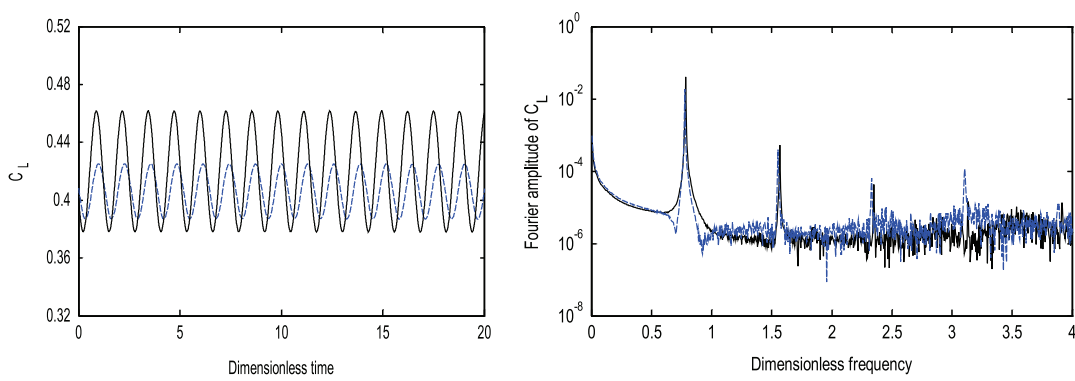


Fig. 5. (Left) Comparison of the time evolutions of the lift coefficient for the flat plate at an incidence of 10° without (solid, black curve) and with (blue dashed curve) a poro-elastic coating; (right) comparison of the Fourier spectra of the lift coefficients shown in the left frame – the legends (colour codes) are same as for the left frame. (For interpretation of the references to colour in this figure caption, the reader is referred to the web version of this paper.)

The left frame of Fig. 4 illustrates that the first reference feather (which is closest to the leading edge of the plate) has some oscillatory dynamics, while the other three reference feathers are always aligned with the free-stream (which is also set as the initial condition for the angular dynamics of the reference feathers, while running the simulations). Further, from the right frame of Fig. 4, it can be seen that the frequency distribution exactly concurs with that shown in Fig. 3. Thus, the fluid and the structure parts oscillate with exactly the same frequency equal to 0.4947, which is slightly modified from the inherent structural frequency equal to 0.4594, as calculated towards the beginning of this section. Hence, the dynamics of the structure part dictates the dynamics of this coupled fluid–structure system, for this flow case.

Case B: Flat plate oriented at an angle to the free-stream. Now, a plate oriented at an angle equal to 10° to the free-stream is considered. The left and right frames of Fig. 5 show a comparison of the dynamics of the lift coefficient for this plate without and with coating.

From the solid black curve in the right frame of Fig. 5, it can be seen that the Fourier spectrum for a smooth, tilted flat plate has a *unique* fundamental frequency (coinciding with the frequency of vortex-shedding) equal to 0.7831, along with all its super-harmonics. This frequency is inherently associated with the characteristics of the flow over the plate. Now, when this plate is covered with a poro-elastic coating (with exactly the same physical and structural parameters as for the case of the horizontal plate), it can be seen from Fig. 5 that the lift oscillations have substantially decreased, together with a small reduction in the mean value of lift. This can also be seen from the amplitude of the fundamental frequency, as shown by comparing the blue and black curves in the right frame of Fig. 5. Further, by analyzing the dashed curve here, one sees that there is a *unique* fundamental frequency, now equal to 0.7767, along with all its super-harmonics. This frequency is but a mild modification of the vortex shedding frequency 0.7831 in the absence of coating. This frequency modification is the result of energy being dissipated because of damping introduced by the coating, analogous to the frequency modification arising due to the linear damping term in a single degree-of-freedom linear harmonic oscillator.

Fig. 6 shows the dynamics of the four reference feathers approximating the coating, both in the time and frequency domains. From the left frame of Fig. 6, it can be seen that the dynamics of the reference feathers become progressively more violent (that is, more oscillatory in nature) as they approach the end of the top side of the flat plate. This can also be seen from the right frame of Fig. 6, which shows the frequency distribution. Further, in each of the cases of the four reference feathers, sharp amplitude peaks can be seen at values of 0.7767, followed by smaller peaks at its super-harmonics. This is

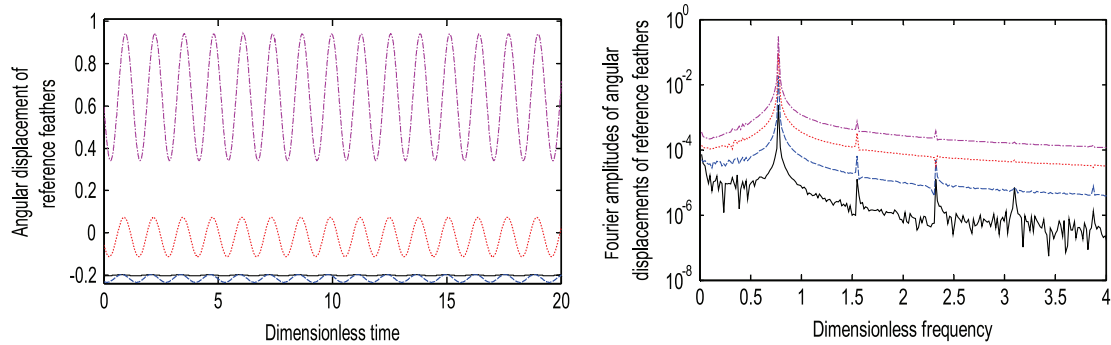


Fig. 6. (Left) Time evolution of the angular displacement of the reference feathers, corresponding to the case shown in Fig. 5 (i.e., for the flat plate at an incidence of 10°). The black solid, blue dashed, red dotted and pink dash-dotted curves show the dynamics of feathers 1, 2, 3 and 4, respectively; (right) Fourier spectra of the angular displacement of the reference feathers, shown in the left frame – the legends (colour codes) are same as for the left frame. (For interpretation of the references to colour in this figure caption, the reader is referred to the web version of this paper.)

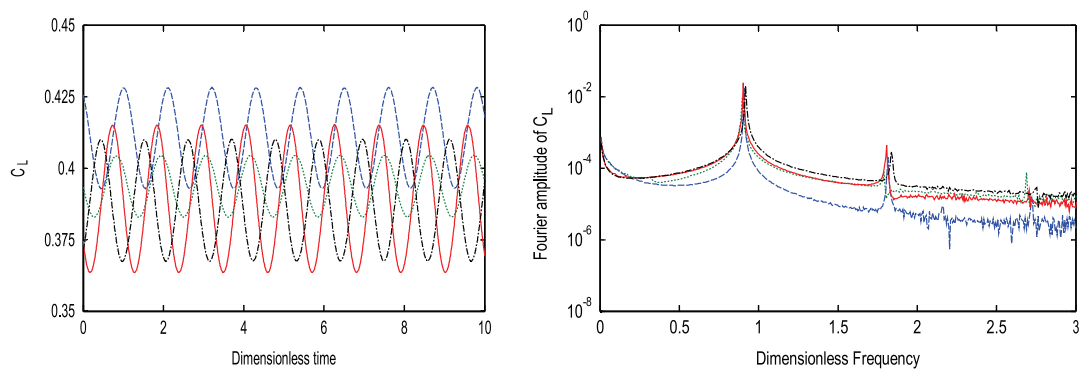


Fig. 7. (Left) Time evolution of the lift coefficient for aerofoil at 10° angle of attack, with poro-elastic coating where the rigidity frequency ω_r is set equal to half the frequency of vortex-shedding; (right) Fourier amplitudes corresponding to the time signals shown in the left frame. This figure shows three cases of placements of the poro-elastic coating on the suction side of the aerofoil: (a) last 30% of the suction side (green dotted curve); (b) first 70% of the suction side (blue dashed curve); and (c) first 50% of the suction side (red solid curve). The black dash-dotted curve shows the reference case, i.e. aerofoil without any coating. (For interpretation of the references to colour in this figure caption, the reader is referred to the web version of this paper.)

exactly the same frequency obtained from the Fourier spectrum of the lift coefficient, shown in Fig. 5. Hence, the dynamics of this coupled system is governed by that of the fluid part.

The fluid component that governs the dynamics of the coupled system need not always be the case. The magnitude of the effect can vary, essentially with the characteristics of the coating. However, the case considered in the present section gives useful insight into how structure parameters can be selected to modify the dynamics of the coupled system in desired ways. As will be outlined in the next sub-section, which presents results for a poro-elastically coated aerofoil, the influence of the coating can be strong enough to show its presence in both the frequency spectra of the lift coefficient as well as the dynamics of the coating (i.e., the dynamics of the fluid part and the structure part), an instance of this being the presence of damped peaks corresponding to the structure frequency.

4.2. Case of symmetric aerofoil

Various simulations were performed for a poro-elastically coated aerofoil at 10° angle of incidence to the free-stream, with different structural as well as physical parameters (such as the rigidity frequency, the length of reference feathers, and the placement of the coating on the aerofoil – cf. Venkataraman and Bottaro, 2012). It was observed that in none of these cases, the dynamics of either the fluid or the structure systems (as captured by the quantities $C_L(t)$ and $\theta(t)$) exhibited the characteristics shown in case 2, i.e., the case in which the Fourier decomposition of the dynamics (of both fluid as well as structure) showed exactly one frequency $\omega_{s,2}$ without any super-harmonics. Further, from the perspective of the dynamics of the fluid component, all the simulation results from the computational model could be classified into cases 1 and 3 (as explained in Sections 2 and 3). That is, either the case was that the dynamics of the fluid system showed a fundamental frequency $\omega_{s,1}$ and its super-harmonics and the structure system showed the same fundamental frequency (such as the coated flat plate case presented in the previous sub-section), or the dynamics of the fluid and structure systems showed two unrelated frequencies $\omega_{s,1}$ and $\omega_{s,2}$ along with super-harmonics of the frequency $\omega_{s,1}$.

The left frame of Fig. 7 shows the steady-state time evolution of the lift coefficient of the aerofoil $C_L(t)$ for three cases of coatings, for each of which the angular rigidity frequency ω_r (which is also taken to be the dominant structure frequency) is set to the value 2.8972, which is half of the fundamental frequency in the fluid system ω_f (which in turn is the frequency of

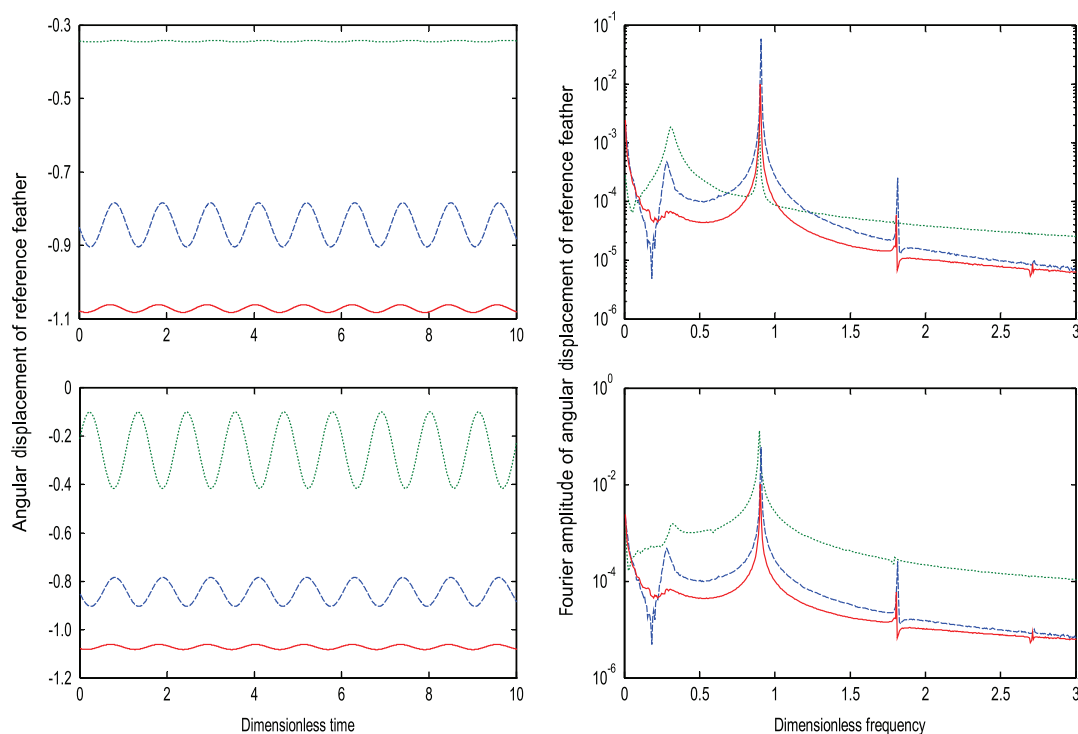


Fig. 8. (Left) Time evolutions of the angular displacement of (top) the reference feather near the middle of the suction side, and (bottom) the reference feather nearest to the trailing edge, for the cases shown in Fig. 7 (i.e., for an aerofoil at 10° angle of attack with different placements of the poro-elastic coating); (right) respective Fourier amplitudes corresponding to the time signals shown in the left frames.

vortex-shedding – cf. Venkataraman, 2013, Venkataraman et al., 2013). Three cases of placements of the coating have been illustrated here, where the suction side is covered on the first 50%, the first 70%, and the end 30% of its length.

At this point, it must be noted that the lift coefficients of a flat plate as well as an aerofoil, both at an incidence of 10° , either without or with coating, are within the same range of time-averaged mean values. However the vortex-shedding frequencies in both these cases are different (being around 0.75 and 0.9). This difference (which can also be seen from the frequency spectra of both – as shown in the right frames of Figs. 5 and 7) is possibly intrinsic to the differences in the shape of the two bodies.

The right frame of Fig. 7 shows the Fourier decomposition for these three cases. In each of these cases, a sharp peak at certain *unique* frequencies is observed, followed by peaks with amplitude of smaller magnitudes at twice and thrice these frequencies. In addition, for the case in which the end 30% of the aerofoil's suction side is poro-elastically coated (i.e., the green dotted curve), a small *damped* frequency peak can also be seen at another frequency equal to 0.3087 (corresponding to the angular frequency of 1.9396). Thus, in this case the coating is strong enough to show its presence in the coupled dynamics. Also, this case corresponds to case 3 (i.e., when the dissipation constant of the reference feather c is zero, and the lift has a non-zero steady-state amplitude), while the other two cases correspond to case 1 (i.e., when the reference feather has zero steady-state amplitude for its angular displacement, and the lift has a non-zero steady-state amplitude), both these cases explained in detail in Section 2.

The left frames of Fig. 8 (both top as well as bottom) show the steady-state time evolution of the angular displacement of a certain reference feather for the three cases of coating shown in Fig. 7. From the right frames of Fig. 8 (both top as well as bottom), which show the Fourier decompositions of the top-left and bottom-left frames of Fig. 8, it can be clearly seen (from the red solid curve) that, for this rigidity frequency, when the extent of the coating is only over the first half of the suction side (i.e., an area over which there is possibly not much interaction of the poro-elastic coating with the vortex-shedding from the trailing edge), the fluid and the structure systems oscillate at the same *unique* frequency $\omega_{s,1}$. However, when the extent of the coating either crosses or shifts to the later half of the suction side, the dynamics of both the fluid and structure systems become progressively richer, with the appearance of new frequencies, such as the *damped* frequency peak $\omega_{s,2}$ of value equal to 1.9396 ($= 2\pi \times 0.3087$) respectively for the blue dashed and green dotted curves appearing because of the structure part.

5. Comparison with results from computational model

From all the simulations performed with the computational model for the symmetric NACA0012 aerofoil with different characteristics of coating, super-harmonics of some fundamental frequency were seen at least in the time evolution of the lift coefficient. However, only in case 2 presented in Section 2, it can be clearly seen that the closed-form solution for the lift coefficient does not exhibit any super-harmonics. Hence, for the derivation of the parameters of the minimal model in terms

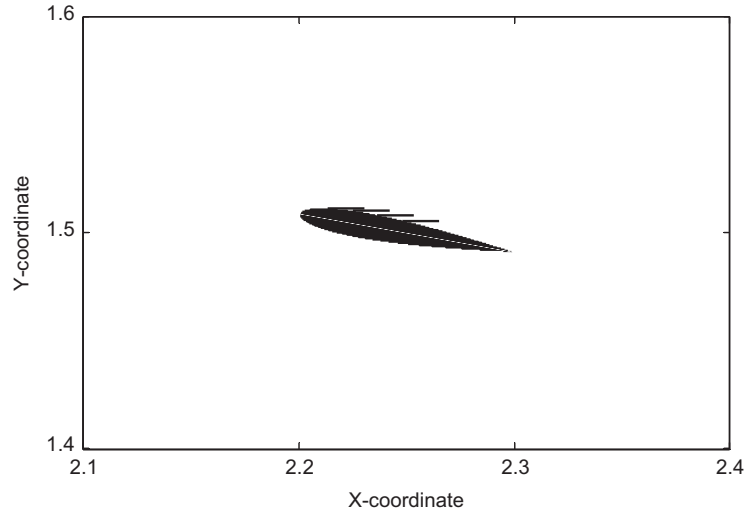


Fig. 9. Placement of the poro-elastic coating over the first 50% of the suction side of the aerofoil, depicted by the position of four reference feathers (shown here by the thick black lines near the leading edge of the aerofoil).

of the characteristics of the results from the computational model (just as it was done for the case of smooth aerofoil, cf. Venkataraman, 2013), two illustrative cases that correspond to cases 1 and 3 of Section 2 are selected. In these two cases, the first 50% and the first 70% of the suction side of the aerofoil are poro-elastically coated, and various aspects of the results from the computational model are shown by the red solid and blue dashed curves in each of the frames in Figs. 7 and 8. The position of the reference control elements on the aerofoil, for the first case, is shown in Fig. 9.

It can be clearly seen from the red solid curve in the right frame of Fig. 7 that, for the lift coefficient, after a peak at the fundamental frequency $\omega_{s,1}$ (which is also the *unique* frequency present in the coupled system), there is a peak with substantial (but smaller) amplitude at $2\omega_{s,1}$ (followed by a further smaller peak at $3\omega_{s,1}$). Hence, as mentioned before, this figure shows a clear correspondence with case 1 explained in Section 2, i.e., the case of *weak structure-to-fluid coupling*.

From the right frame of Figs. 7 and bottom-right frame of Fig. 8, one gets the following values for the fundamental frequency $\omega_{s,1}$, amplitudes of the lift coefficient corresponding to the fundamental frequency and its second and third superharmonics l_1 , l_2 and l_3 respectively; and amplitude of the angular displacement of the reference feather (closest to the trailing edge) ϕ'_1 corresponding to the fundamental frequency:

$$\begin{aligned} \omega_{s,1} &= 2\pi \times 0.9039 = 5.6794; & l_1 &= 0.0245; & l_2 &= 4.459 \times 10^{-4}; \\ l_3 &= 8.123 \times 10^{-6}; & \phi'_1 &= 0.01003. \end{aligned} \quad (5.1)$$

From this value of ϕ'_1 and the known value of the length of the feather, one can evaluate the vertical displacement of the coating interface $\theta'_1 = 8.551 \times 10^{-7}$. Further, $\omega_{s,2}$, l'_1 and θ_1 vanish. Substituting these values in Eqs. (3.3)–(3.10), we get the following values of the parameters for Eqs. (2.3) and (2.4)

$$\begin{aligned} \omega &= 5.6907; & \delta\mu &= 0.0453; & \delta\alpha &= 3.106; \\ \delta\beta &= 4.4571; & \omega_1 &= 0; & \delta\rho_1 &= 0; & \delta\rho_2 &= -1.13 \times 10^{-3}. \end{aligned} \quad (5.2)$$

It must be recalled that for this case, the dissipation constant c of the reference feather is allowed to be arbitrary, and hence can be taken to be arbitrarily large, in line with the physical consideration that the steady-state amplitude a_2 of the *stand-alone* structure part of the coupled system is zero. Such a large value of c is also in line with the fact that the spring constant of the feather/poro-elastic coating ω_1 is zero, which physically means that once the feather is displaced from its initial equilibrium position (for instance, in the process of an initial transient), the *intrinsic* “spring-like” restoring force is not strong enough to bring the feather back to its equilibrium position. A physical example of visualizing this situation could be the case in which the feathers *eventually* align with the free-stream (and hence, the coating has zero displacement in the steady-state). Finally these values of c and ω_1 are also in line with the fact that the structure-to-fluid coupling parameter $\delta\rho_1 = 0$, implying that the structure-to-fluid coupling is *weak*. This conclusion can be easily reconciled with, because the stand-alone *structure oscillator* understandably would not have any effect on the stand-alone *fluid oscillator* in the long run, since its steady-state amplitude (given by a_2 as in Section 2) is zero.

Thus, substituting the values obtained in Eq. (5.2) and by numerically solving it, we can compare this solution with the results from the full computational model, as done in Fig. 10. It can be seen that the results from the computational model and results from the minimal model agree well with each other, in the time as well as frequency domains.

As a second illustration, the case where the first 70% of the suction side of the aerofoil is poro-elastically coated is considered – the position of the reference control elements on the aerofoil is shown in the left frame of Fig. 11. It must be noted here that, from the left frame of Fig. 7, the lift coefficient for the poro-elastically coated aerofoil not only has reduced fluctuations about its mean but also has a higher value of time-averaged mean, as compared to the reference case of an

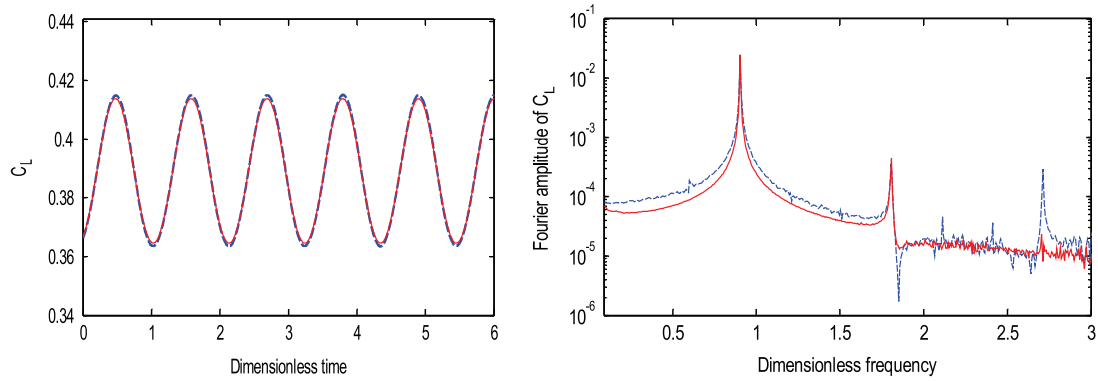


Fig. 10. Comparison of results from minimal model and computational model, for the lift coefficient in (left) time and (right) frequency domains. This case corresponds to the first 50% of the suction side of the aerofoil being poro-elastically coated. The blue dashed curve shows the results from computational model (Venkataraman and Bottaro, 2012) while the red solid curve shows results from the present minimal model. (For interpretation of the references to colour in this figure caption, the reader is referred to the web version of this paper.)

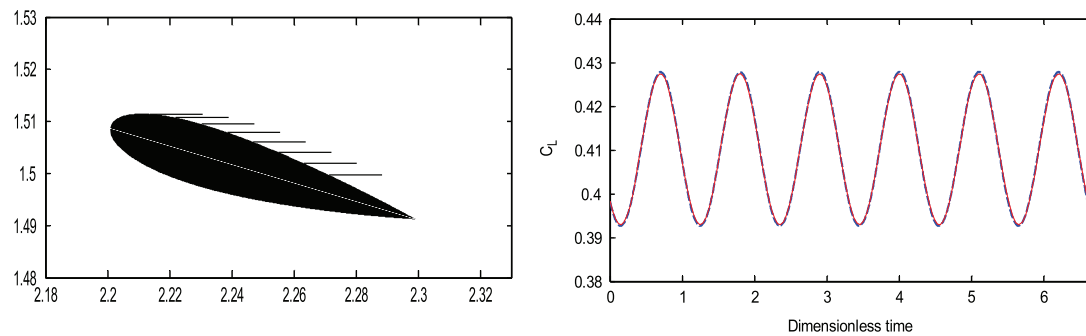


Fig. 11. (Left) Placement of the poro-elastic coating over the first 70% of the suction side of the aerofoil, depicted by the position of reference feathers (shown here by the thick black lines starting from the leading edge of the aerofoil); (right) comparison of results from minimal model and computational model, for the lift coefficient. The blue dashed curve shows the results from computational model (Venkataraman and Bottaro, 2012) while the red solid curve shows results from the present minimal model. (For interpretation of the references to colour in this figure caption, the reader is referred to the web version of this paper.)

aerofoil *without* any coating. From the blue dashed curves shown in the right frames of Figs. 7 and 8, one can deduce that this case shows a correspondence with case 3 explained in Section 2, i.e., the case of **two-way coupling**. Analogous to the first illustrative case, from the frames of Figs. 7 and 8, one can extract the values of the frequencies $\omega_{s,1}$ and $\omega_{s,2}$, amplitudes of the lift corresponding to these two frequencies (i.e., l_1 , l_2 , l_3 and l'_1); and amplitudes of the angular displacement of the reference feather (closest to the trailing edge) for these two frequencies ϕ'_1 and ϕ_1 . With these *input* values substituted in Eqs. (3.3)–(3.10), we recover the values of the parameters for Eqs. (2.3) and (2.4). Substituting these values in the coupled system (Eqs. (2.3) and (2.4)) and by numerically solving it, we can compare this solution with the results of the minimal model, as done in the right frame of Fig. 11.

It can thus be seen that for this case also, the results from the computational model and those from the minimal model agree well with each other. Finally, it must be recalled that for this case, the dissipation constant c of the reference feather is 0, in line with the physical consideration that the steady-state amplitude a_2 of the *stand-alone* structure part of the coupled system is non-zero.

It can also be easily verified that the steady-state solution is independent of the initial conditions (Venkataraman, 2013). All these results indicate the effectiveness of the reduced-order model for vortex-shedding behind a poro-elastically coated aerofoil.

6. Parametric studies for regime changes of coupled system

From the closed-form solution derived for the limit cycle of the dynamical system (2.3)–(2.4), it is possible to illustrate the ranges of *structure* model parameters and the three regimes of weak *fluid-to-structure*, weak *structure-to-fluid* and *two-way* couplings. In this paper, the space which is analyzed is three dimensional and parametrized by the stiffness constant of the coating ω_1 , structure-to-fluid coupling parameter ρ_1 and fluid-to-structure coupling parameter ρ_2 . The latter two parameters can be interpreted as (functions of) density and compliance of the coating, as outlined in Section 2.

Instances of prediction of these parameter regimes are illustrated in this section. For instance, $\omega_{s,2}$ (i.e., the frequency that occurs owing to the structure oscillator (given by equation (2.4))), as a function of the coupling parameters ρ_1 and ρ_2 shown here in Fig. 12, shows a behaviour that is symmetric about the rays $y=x$ and $y=-x$. Further there is a very steep gradient in the magnitude of $\omega_{s,2}$ far away from the origin, but as the values of the coupling parameters approach the origin, this

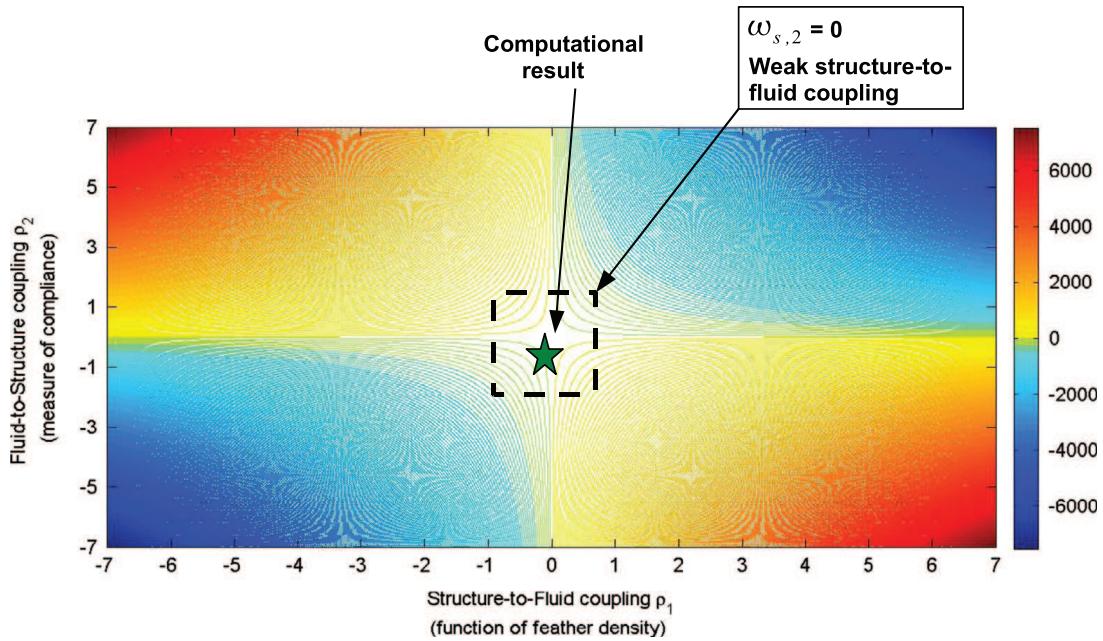


Fig. 12. Dependence of the frequency $\omega_{s,2}$ on the coupling parameters, ρ_1 and ρ_2 respectively, as given in Section 2, when the coefficient of restoring force ω_1 is fixed to the value 10^{-4} (i.e., close to 0 as given by Eq. (5.2)). The star shows the parameters at which the minimal coupled model yields the solution that matches with the computational results for the case of weak structure-to-fluid coupling, as shown in Fig. 10.

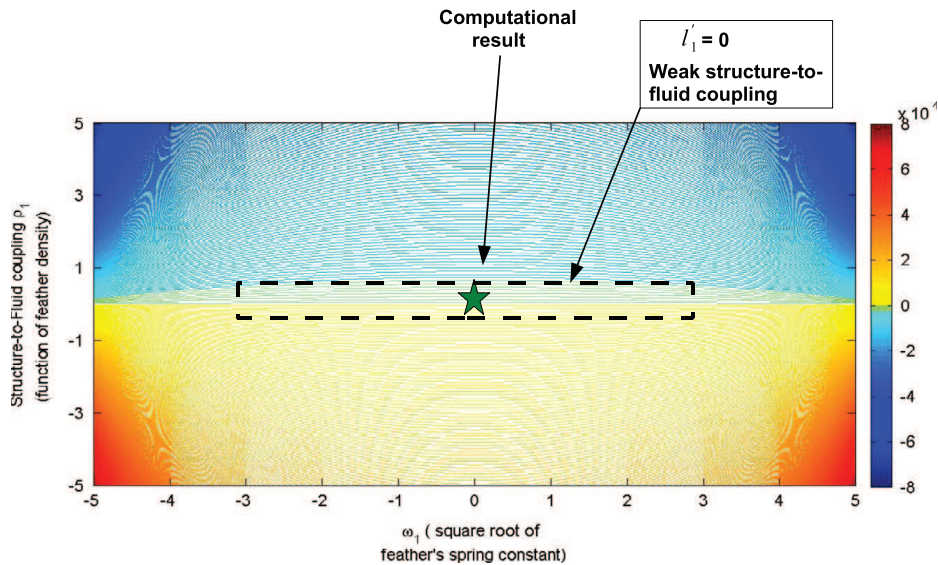


Fig. 13. Dependence of the amplitude l'_1 on the spring constant of the feather ω_1 and the structure-to-fluid coupling parameter ρ_1 , as given by Eqs. (2.16) and (3.1), when the fluid–structure coupling parameter ρ_2 is fixed to the value -1.13×10^{-3} (as given by Eq. (5.2)). The star shows the parameters at which the minimal coupled model yields the solution that matches with the computational results for the case of weak structure-to-fluid coupling, as shown in Fig. 10.

gradient becomes very shallow. A direct consequence of such a behaviour is that the regime of *weak structure-to-fluid coupling* (which also contains parameters for which $\omega_{s,2}$ is zero) is a very small region, as also highlighted in Fig. 12. A similar analysis of the amplitude l'_1 (i.e., the amplitude in the lift coefficient corresponding to the frequency $\omega_{s,2}$) as a function of the spring constant of the poro-elastic coating ω_1 and the structure-to-fluid coupling parameter ρ_1 reveals a behaviour that is symmetric about the vertical (y -)axis. The magnitude of this amplitude sharply drops as the parameter values of (ω_1, ρ_1) approach the horizontal (x -)axis. Such a behaviour again highlights that the regime of *weak structure-to-fluid coupling* is a very narrow band, as in Fig. 13.

7. Conclusions

In this paper, a minimal model for vortex-shedding behind a symmetric aerofoil at an angle of incidence to the free-stream, with a poro-elastic coating on a part of its suction side, has been developed in terms of the unsteady lift coefficient.

To achieve this, the minimal-order model for the vortex-shedding behind a smooth aerofoil has been linearly coupled with a linear damped oscillator for the dynamics of the poro-elastic coating.

For this coupled non-linear model for the lift coefficient, a closed-form expression for its limit cycle is derived in terms of generic (unknown) fluid, structure and coupling parameters (similar to the analysis done for the case of smooth aerofoil). In the course of this analysis, three physical cases could be segregated, based on the possibilities of whether the steady-state amplitudes of the stand-alone *fluid oscillator* (as captured from the dynamics of the lift coefficient) and the stand-alone *structure oscillator* (as captured from the dynamics of fluid-coating interface) were zero or not, and various permutations of these possibilities. For each of these three cases, the expressions for model parameters in terms of the computational features were derived. These closed-form expressions yielded conditions on resonant and non-resonant regimes of fluid and structure frequencies, thus giving an insight into possible selection of structure and coupling parameters that are capable of yielding, for instance, reduced lift fluctuations, as compared to the case of the smooth aerofoil.

Several simulation results for coated aerofoils, with different extents and placements of coating over the suction side, are presented, and all these solutions from the full computational model are seen to fall in one of the two cases of possible values for steady-state amplitudes. Based on this observation, the various characteristics of the periodic solution obtained from the computational model are compared with the corresponding characteristics of the closed-form solution for the limit cycle obtained from the minimal model. From this, the fluid, structure and coupling parameters, that yield matching of trajectories obtained from the minimal model and computational model, are determined. All the above observations indicated the effectiveness of the minimal model for poro-elastically coated aerofoils.

During the course of this research, the following problem areas were identified as potential topics for future work:

- (a) The minimal model for the poro-elastic coating is purely linear (although it reproduces results very well from the computational model and provides valuable insights in selecting optimal parameters for the coating).
- (b) The structure–fluid and fluid–structure coupling terms considered here are linear.

One consequence of considering a *linear minimal* model for the structures, as summarized above, is that interaction effects between neighbouring reference feathers are neglected in an *average* sense (by employing the structure model to study the dynamics of only the fluid-coating interface), or the case where all feathers are sufficiently far apart, to be able to meaningfully visualize a scenario with identical and synchronous dynamics for each structural element. Hence, possible extensions can be made to formulate progressively non-linear models for the structure and coupling parts, to more realistically approximate such a poro-elastic coating and to also be able to trust its effectiveness for different flow regimes.

Acknowledgements

Part of the work of the first author has been conducted as a Visiting doctoral student at the Jawaharlal Nehru Centre for Advanced Scientific Research, Bangalore, India and the Centre for Interdisciplinary Sciences, Tata Institute of Fundamental Research, Hyderabad, India. The financial support received from both these places is gratefully acknowledged.

References

- Bakhtian, N.M., Babinsky, H., Thomas, A.L.R., Taylor, G.K., 2007. The low Reynolds number aerodynamics of leading edge flaps. In: Proceedings of the 45th AIAA Aerospace Sciences Meeting and Exhibit, Reno, NV, pp. 8018–8030.
- Bechert, D.W., Bruse, M., Hage, W., Meyer, R., 1997. Biological Surfaces and Their Technological Application—Laboratory and Flight Experiments on Drag Reduction and Separation Control. AIAA paper No. 97-1960.
- Brücker, C., 2011. Interaction of flexible surface hairs with near-wall turbulence. *Journal of Physics: Condensed Matter* 23, 184120. (special issue on Nano- and Microfluidics).
- Brücker, C., Weidner, C., 2013. Separation control via self-adaptive hairy flaplet arrays. In: Proceedings of the ERCOFTAC International Symposium on Unsteady Separation in Fluid-Structure Interaction, Mykonos, Greece.
- Currie, I., Turnbull, D., 1987. Streamwise oscillations of cylinders near the critical Reynolds number. *Journal of Fluids and Structures* 1 (2), 185–196.
- Favier, J., Dauphin, A., Basso, D., Bottaro, A., 2009. Passive separation control using a self-adaptive hairy coating. *Journal of Fluid Mechanics* 627, 451–483.
- Gaster, M., 1969. Vortex shedding from slender cones at low Reynolds numbers. *Journal of Fluid Mechanics* 38 (3), 565–576.
- Hartlen, R., Currie, I., 1970. Lift-oscillator model of vortex-induced vibration. *ASCE Journal of Engineering Mechanics* 96 (5), 577–591.
- Igbalajobi, A., McClean, J.F., Sumner, D., Bergstrom, D.J., 2013. The effect of a wake-mounted splitter plate on the flow around a surface-mounted finite-height circular cylinder. *Journal of Fluids and Structures* 37, 185–200.
- Jang, G.W., Chang, S.M., Gim, G.H., 2013. Fluid-structure interaction of quasi one-dimensional potential flow along channel bounded by symmetric cantilever beams. *Journal of Fluids and Structures* 40, 127–147.
- Lam, K., Lin, Y.F., Zou, L., Liu, Y., 2012. Numerical study of flow patterns and force characteristics for square and rectangular cylinders with wavy surfaces. *Journal of Fluids and Structures* 28, 359–377.
- Perdikaris, P.G., Kaitktsis, L., Triantafyllou, G.S., 2009. Chaos in a cylinder wake due to forcing at the Strouhal frequency. *Physics of Fluids* 21, 101705-1–101705-4.
- Rand, R.H., 2012. Lecture Notes on Non-linear Vibrations. Available at (<http://www.math.cornell.edu/~rand/randdocs>).
- Srikanth, T., Dixit, H.N., Rao, T., Govindarajan, R., 2011. Vortex shedding patterns, their competition, and chaos in flow past inline oscillating rectangular cylinders. *Physics of Fluids* 23, 073603-1–073603-9.
- Strogatz, S.H., 1994. *Nonlinear Dynamics and Chaos*. Addison-Wesley, Reading, MA.
- VanDyke, M., 1964. *Perturbation Methods in Fluid Mechanics*. Academic Press, NY.

- Venkataraman, D., 2013. Flow Control Using a Porous, Compliant Coating of Feather-like Actuators (Ph.D. thesis). Department of Civil, Chemical and Environmental Engineering, University of Genova, Italy. Available at (http://www.dicca.unige.it/bottaro/Presentation%20group/Thesis_DivyaVenkataraman.pdf).
- Venkataraman, D., Bottaro, A., 2012. Numerical modeling of flow control on a symmetric aerofoil via a porous, compliant coating. *Physics of Fluids* 24, 093601-1–0936011-9.
- Venkataraman, D., Marathe, A., Bottaro, A., Govindarajan, R., 2013. Minimal modeling for flow control via a poro-elastic coating. In: Proceedings of the ERCOFTAC International Symposium on Unsteady Separation in Fluid-Structure Interaction, Mykonos, Greece.
- Xu, S.J., Zhou, Y., Wang, M.H., 2006. A symmetric binary-vortex street behind a longitudinally oscillating cylinder. *Journal of Fluid Mechanics* 556, 27–43.